SARS-CoV-2 diverges from other betacoronaviruses in only partially activating the IRE1α/XBP1 ER stress pathway in human lung-derived cells

Long C. Nguyen[1*], David M. Renner[6,9*], Diane Silva[2*], Dongbo Yang[1], Kaeri M. Medina[6], Vlad Nicolaescu[3,10], Haley Gula[3,10], Nir Drayman[4], Andrea Valdespino[1], Adil Mohamed[4], Christopher Dann[1], Kristin Wannemo[2], Lydia Robinson-Mailman[1], Alan Gonzalez[2], Letícia Stock[1], Mengrui Cao[2], Zeyu Qiao[5], Raymond E. Moellering[5], Savas Tay[4], Glenn Randall[3,10], Michael F. Beers[7,8], Marsha R. Rosner[1#], Scott A. Oakes[2#], Susan R. Weiss[6,9#]

[1]Ben May Department for Cancer Research, [2]Department of Pathology, [3]Department of Microbiology, [4]Pritzker School of Molecular Engineering, [5]Department of Chemistry, University of Chicago, Chicago, IL 60637, U.S.A. [6]Department of Microbiology, [7]Department of Medicine, [8]Penn-CHOP Lung Biology Institute, [9]Penn Center for Research on Coronaviruses and Other Emerging Pathogens, Perelman School of Medicine, University of Pennsylvania, Philadelphia, PA 19104, USA. [10]Howard Taylor Ricketts Laboratory, Argonne National Laboratory, Lemont, IL 60439, USA.

* Equal contribution.# Co-corresponding authors: mrosner@uchicago.edu (M.R.R.); soakes@bsd.uchicago.edu (S.A.O.); weisssr@pennmedicine.upenn.edu (S.R.W.);

Summary:

Despite the efficacy of vaccines, severe acute respiratory syndrome coronavirus 2 (SARS-CoV-2) has killed over 5 million individuals worldwide and continues to spread in countries where the vaccines are not yet widely available or its citizens are hesitant to become vaccinated. Therefore, it is critical to unravel the molecular mechanisms that allow SARS-CoV-2 and other coronaviruses to infect and overtake the host machinery of human cells. Coronavirus replication triggers endoplasmic reticulum (ER) stress and activation of the unfolded protein response (UPR), a key host cell pathway widely believed essential for viral replication. We examined the activation status and requirement of the master UPR sensor IRE1α kinase/RNase and its downstream transcription factor effector XBP1s, which is processed through an IRE1α-mediated mRNA splicing event, in human lung-derived cells infected with betacoronaviruses. We found human respiratory coronavirus OC43 (HCoV-OC43), Middle East respiratory syndrome coronavirus (MERS-CoV), and the murine coronavirus (MHV) all induce ER stress and strongly trigger the kinase and RNase activities of IRE1α as well as XBP1 splicing. In contrast, SARS-CoV-2 only partially activates IRE1α whereby it autophosphorylates, but its RNase fails to splice XBP1. Moreover, IRE1α was dispensable for optimal replication in human cells for all coronaviruses tested. Our findings demonstrate that IRE1α activation status differs upon infection with distinct betacoronaviruses and is not essential for efficient replication of any of them. Our data suggest that SARS-CoV-2 actively inhibits the RNase of autophosphorylated IRE1α through an unknown mechanism, perhaps as a strategy to eliminate detection by the host immune system.

Importance.

SARS-CoV-2 is the third lethal respiratory coronaviruses after MERS-CoV and SARS-CoV to emerge this century, causing millions of deaths world-wide. Other common coronaviruses such as OC43 cause less severe respiratory disease. Thus, it is imperative to understand the similarities and differences among these viruses in how each interacts with host cells. We focused here on the inositol-requiring enzyme 1α (IRE1α) pathway, part of the host unfolded protein response to virus-induced stress. We found that while MERS-CoV and OC43 fully activate the IRE1α kinase and RNase activites, SARS-CoV-2 only partially activates IRE1α, promoting its kinase activity but not RNase activity. We propose that SARS-CoV-2 prevents IRE1α RNase activation as a strategy to eliminate detection by the host immune system.

Introduction:

Severe acute respiratory syndrome coronavirus 2 (SARS-CoV-2) emerged in China in late 2019. It was the third lethal zoonotic coronavirus to emerge into humans after SARS-CoV (2002) and Middel East respiratory syndrome coronavirus (MERS-CoV) (2012), each of which has been associated with acute lung injury and hypoxemic respiratory failure. While coronaviruses are divided into four general groups (alpha, beta, gamma and delta)(1, 2), all three of the lethal human coronaviruses are betacoronaviruses, albeit from different lineages (Figure 1A). SARS-CoV and SARS-CoV-2 are sarbecoviruses while MERS-CoV is a merbecovirus. Other human CoVs, including HCoV-OC43 (OC43) and HCoV-HKU1 (HKU-1), are embecoviruses as is the model murine coronavirus mouse hepatitis virus (MHV). All CoVs have similar genome structures, replication cycles, and exhibit tropism for the epithelia of the respiratory tract, the portal of entry. They replicate their RNAs and produce subgenomic mRNAs by conserved mechanisms and encode homologous structural as well as replicase proteins. Despite the similarities among all coronaviruses, each lineage expresses distinct accessory proteins that may confer differences in host-virus interactions. Indeed, we have previously found that SARS-CoV-2, MERS-CoV and MHV all induce somewhat different levels of activation and/or antagonism of interferon (IFN) signaling and other dsRNA induced antiviral innate responses (3-5). We show here that differences in virus-induced host responses can be extended to discrete effects on a key pathway regulating protein homeostasis (proteostasis).

One third of all eukaryotic proteins, including most that are inserted into membranes or secreted, are synthesized through co-translational translocation into the ER lumen. Likewise, viral membrane associated proteins are translated and processed in association with the ER (6, 7). Once in the ER, these polypeptides undergo stringent quality control montoring to ensure that they are properly processed and folded. If the capacity to fold proteins is unable to keep up with demand, misfolded proteins will accumulate in the ER lumen—a condition referred to as “ER

stress." The presence of misfolded proteins in the ER are sensed by three transmembrane sentinel proteins--activating transcription factor 6 (ATF6), PKR-like ER kinase (PERK), and inositol-requiring enzyme 1α (IRE1α)--which trigger an intracellular signaling pathway called the unfolded protein response (UPR). In an effort to restore proteostasis, activation of these sensors induces transcription factors that turn on genes encoding chaperones, oxidoreductases, and ER-associated decay (ERAD) components(8). The UPR also inhibits Cap-dependent translation, thus decreasing the load on the ER and giving it extra time to fold proteins already in production (9, 10). If successful, these adaptive UPR programs restore ER homeostasis.

The most ancient UPR pathway is controlled by IRE1α—an ER transmembrane bifunctional kinase/endoribonuclease (RNase) that employs auto-phosphorylation to control its catalytic RNase function(11, 12). In response to ER stress, IRE1α undergoes auto-phosphorylation and dimerization to allosterically activate its RNase domain to excise a 26nt non-conventional intron in *XBP1* mRNA; re-ligation of spliced *XBP1* shifts the open reading frame, and its translation produces the homeostatic transcription factor XBP1s (s=spliced)(13, 14). Once synthesized, XBP1s upregulates genes that expand the ER and its protein folding machinery (15). IRE1α can additionally lead to apoptosis and inflammation via JUN N-terminal kinase (JNK) and p38 mitogen-activated protein kinase (MAPK) signaling (16). Prolonged ER stress can induce regulated IRE1-dependent decay (RIDD), promoting the cleavage of additional targets beyond XBP1 mRNA, such as secretory protein and ER-localized mRNAs (17). In the short term RIDD may promote adaptation through further reducing translation and protein burden on the ER; however, prolonged RIDD leads to the depletion of vital ER resident enzymes and structural components to exacerbate ER stress and hasten cell death (11, 18) .

There is a large body of evidence that viral replication of mammalian cells can trigger ER stress and UPR activation in infected cells (19), and numerous studies report that the UPR is activated

upon infection of host cells by coronavirus family members (6, 7, 20-23). Coronaviruses induce stress in ER in several ways. First, conserved replicase encoded, non structural proteins nsp3, nsp4 and nps6 are embedded into the ER membrane, and along with unknown host factors, promote membrane curvature to form double memebrane vesicles (DMVs), the site of viral replication and transcription centers. In addition to taking over the ER, coronaviruses further condition infected cells by shifting translation away from host mRNAs and instead to viral mRNAs. Translation of viral mRNAs casues the ER, already depleted of membranes, to be flooded with heavily glycosylated viral structural proteins (e.g., spike (S), membrane (M) and envelope (E)), challenging the organelle's folding capacity and overall integrity. Finally, cell membranes are depleted as enveloped virus particles are asembled into new virions in the ER-Golgi intermediate compartment before budding from the infected cell (1). Thus, coronaviruses as well as other enveloped viruses promote a massive ER expansion and modification necessary to replicate their genomes, transcribe mRNAs, and finally to process and package their protein products into viral particles.

In this study, we have compared the activation status and requirement of the IRE1α/XBP1 arm of the UPR in well-characterized human lung epithelial cell lines and in induced pluripotent stem cell (iPSC)-dervied type II alveolar (iAT2) cells. following infection with four betacoronaviruses representing three distinct lineages. We find that infection with MERS-CoV, HCoV-OC43 and MHV leads to phosphorylation of IRE1α and the consequent production of spliced XBP1 transcription factor. Surprisingly, while we observed phosphorylation of IRE1α in SARS-CoV-2 infected cells, there was notable absence of XBP1s, suggesting SARS-CoV-2 inhibits downstream signaling of the IRE1α/XBP1 arm of the UPR.

RESULTS

Induction of IRE1α phosphorylation following coronavirus infection.

To determine whether betacoronaviruses activate IRE1α, we first examined the level of phosphorylated IRE1α after viral infection of the A549 human lung carcinoma cell line. We used A549 cells stably expressing the following receptors to facilitate optimal entry for each of the viruses: carcinoembryonic antigen cell adhesion molecule (CEACAM)1a or MHVR (MHV), dipeptidyl peptidase DPP4 (MERS-CoV), or angiotensin converting enzyme (ACE)2 (SARS-CoV-2). HCoV-OC43 can infect parental A549 or cells expressing ACE2 (3). Consistent with previous reports that embeco lineage coronaviruses MHV (20, 24) and OC43 (25) induce ER stress, we observed a significant increase in phospho-IRE1α (p-IRE1α) during infection by either HCoV-OC43 (24 or 48hpi) or MHV (24hpi) (Figure 2A-C). To confirm the specificity of the p-IRE1α band, we pretreated cells prior to infection with KIRA8, a highly selective kinase inhibitor of IRE1α inhibitor known to inhibit both autophosphorylation and consequently RNase activity. As expected, KIRA8 significantly inhibited the induction of p-IRE1α by OC43 and MHV (Figure 2A&C). Thapsigargin (Tg) and tunicamycin (Tm), both inducers of ER stress, were used as further controls (Figure 2B,D&E). Robust induction of p-IRE1α was observed with 1 hour of Tg (1μM) treatment; while no activation of p-IRE1α was observed after 8 hours of treatment with Tm (1μg/ mL), consistent with the negative feedback regulation observed with extended Tm treatment (26). We also observed robust phosphorylation of IRE1α in A549-DDP4 cells and A549-ACE2 cells infected by MERS-CoV and SARS-CoV-2, respectively at 24 and 48 hpi (Figure 2D-F and S1A&B). As with OC43 and MHV, IRE1α phosphorylation during SARS-CoV-2 infection was inhibited by KIRA8 (Fig 2F). These results are not limited to a single cell type as we observed similar induction of p-IRE1α in Calu-3 cells, which can be productively infected with both MERS-CoV or SARS-

CoV-2 (Figure 2G). These results demonstrate that MERS-CoV and SARS-CoV-2, like OC43 and MHV, activate the host IRE1α kinase after infection.

MHV, OC43, MERS-COV but not SARS-COV-2 induce splicing of XBP1 mRNA.

We next examined the effect of coronavirus infection on the RNase activity of IRE1α as assessed by XBP1 splicing. Using specific primers to quantify spliced XBP1 mRNA (XBP1s), we observed a marked increase in the percent of spliced XBP1 mRNA (% XBP1s) as well as an increase in the relative amount of spliced XBP1 mRNA (XBP1s) compared to mock control after infection by OC43, MERS-CoV or MHV in receptor-expressing A549 cells (Figure 3A&B and S2A&B). This induction of XBP1s by OC43 and by MERS-CoV infection was confirmed by assessing XBP1 splicing by agarose gel electrophoresis (Figure 3E&F). DNAJB9, a canonical target of XBP1s, was also markedly upregulated with OC43, MERS-CoV, and MHV infection at both 24 and 48 hours post-infection (Figure 3A&B and S2B). This induction of IRE1α RNase activity is coincident with the observed autophosphorylation of p-IRE1α upon OC43, MHV or MERS-CoV infection.

Surprisingly, despite the observed IRE1α autophosphorylation following SARS-CoV-2 infection, there was no significant upregulation of XBP1s mRNA in A549-ACE2 cells up to 52 hours post-infection (Figure 3C&G). Similarly, DNAJB9 expression levels were unchanged at all time points observed with SARS-CoV-2 (Figure 3C). To confirm this effect is not limited to A549 cells, we measured XBP1 mRNA splicing in MERS-CoV and SARS-CoV-2-infected Calu-3 cells. Again, infection with MERS-CoV, but not SARS-CoV-2, significantly induced XBP1s and its downstream effector DNAJB9 (Figure 3D&H). In agreement with the RNA results, OC43, but not SARS-CoV-2, infection induced XBP1s protein levels (Figure 3I&J).

MHV, OC43, MERS-COV but not SARS-CoV-2 induce UPR related genes upon infection.

To determine how different coronaviruses impact the UPR at the transcriptional level, we performed RNA-sequencing of A549-DPP4 cells infected with MERS-CoV for 24 and 36 hours and compared the results to published RNA-seq data sets (24, 27) of MHV infection of murine bone marrow derived macrophages (BMDM) or SARS-CoV-2 infection of A549-ACE2, normal human bronchial epithelial (NHBE) cells, and Calu-3 cell lines. In agreement with our IRE1α activation results, Ingenuity Pathway Analysis (IPA) predicted activation of the UPR and ER stress pathways by MERS-CoV and MHV (Figure 4A). In contrast, SARS-CoV-2 consistently showed no activation and even a slight inhibition of the UPR and ER stress pathway across different MOI conditions and cell lines.

To support the results of the gel electrophoresis splicing assays for XBP1 mRNA that distinguished SARS-CoV-2 infection from that of the other betacoronaviruses (Figure 3), we further utilized the RNA sequencing results to quantitatively measure XBP1 mRNA splicing by these coronaviruses. Through RNA-seq, we visualized both the unspliced and spliced XBP1 mRNA reads based on whether they contain the 26 nucleotide non-conventional intron that is removed as a result of RNase activity of IRE1α (Figure 4B&C). MERS-CoV infection resulted in significant XBP1 mRNA splicing, in contrast with no difference detected in SARS-CoV-2 infected versus mock-infected cells (Figure 4B&C). We further quantified total XBP1 spliced vs unspliced reads, which consistently showed a substantial increase in the percent expression of the XBP1s reads when normalized to total XBP1 reads for MERS-CoV at both 24 and 36 hours post-infection but not for SARS-CoV-2 infected cells (Figure 4D&E), consistent with significant upregulation of DNAJB9 and total XBP1 during infection with MERS-CoV but not SARS-CoV-2 (Figure 4F-I).

MERS-CoV but not SARS-CoV-2 induces XBP1 splicing during infection of biologically relevant iPSC-derived alveolar type II cells

To confirm our results in a more physiologically relevant cell, we obtained iPSC-dervied type II alveolar (iAT2) cells. We employed the SPC2 line, which expresses tdTomato from the surfactant protein-C (SFTPC) locus as an AT2 marker, that we have previously used to characterize innate immune responses to SARS-CoV-2 infection (3). Type II alveolar cells are a major target during both MERS-CoV and SARS-CoV-2 infection in humans, and their destruction may be a contributing factor to lung pathogenesis in severe cases (28, 29).

Both MERS-CoV and SARS-CoV-2 replicate in these cells and release infectious virus as quantified by plaque assay (Figure 5A). Notably, MERS-CoV replicated to higher titers than SARS-CoV-2 in these lung derived cells. This complements our previous findings that SARS-CoV-2 replicates more efficiently than MERS-CoV in upper respiratory derived primary nasal cells (3) and may reflect that MERS-CoV is better adapted to replicating within the lower respiratory tract while SARS-CoV-2 replicates more efficiently in the upper airway. Despite this difference in replication, both viruses were observed to induce p-IRE1α over the course of infection (Figure 5B). In agreement with our results in A549 and Calu-3 cells, SARS-CoV-2 failed to induce XBP1 splicing in iAT2 cells, as measured by RT-qPCR (Figure 5C). Contrasting this, MERS-CoV induced XBP1 splicing, albeit to a lower extent than in immortalized cell lines. Lastly, we visualized XBP1 splicing using RT-PCR and agarose gel electrophoresis (Figure 5D). Again, our data indicate that SARS-CoV-2 fails to induce XBP1 splicing at either 24 or 48hpi in iAT2 cells, despite inducing p-IRE1α. MERS-CoV, however, induced increasing XBP1 splicing over the course of infection, matching the results in A549 and Calu-3 cells (Figures 2 and 3). Overall, these results indicate that both SARS-CoV-2 and MERS-CoV induce ER stress as evidenced by IRE1α phosphorylation during infection of primary iAT2 cells, but only MERS-CoV induces the downstream effects of active IRE1α RNase.

SARS-CoV-2 inhibits XBP1 splicing

We then tested whether SARS-CoV-2 actively inhibits splicing of XBP1 induced by glycosylation inhibitor tunicamycin (TM), a common agent used to chemically induce ER stress. To do so, A549-ACE2 cells were either mock infected or infected with SARS-CoV-2 or OC43 for 24 hours and then treated with TM for 6 hours prior to analysis. Interestingly, while SARS-CoV-2 infection did not completely prevent XBP1 splicing induced by TM, it led to significantly lower XBP1 splicing levels compared with mock infected cells (Figure 6A). In contrast, OC43 increased further XBP1 splicing at all used concentration of TM (Figure 6B). This result suggests that SARS-CoV-2 actively inhibits RNase activation IRE1α.

Betacoronaviruses do not require IRE1α for replication

Given the presumed importance of IRE1α/XBP1s to expand the ER and maintain protein folding during viral replication, and the interesting differences we observed between SARS-CoV-2 and the other betacoronaviruses, we next explored the consequences for its inhibition on the replication of each. To determine whether IRE1α activity is required for replication and propagation of MHV, HCoV-OC43, MERS-CoV or SARS-CoV-2, we utilized CRISPR/Cas9 gene editing to knock out IRE1α in A549 cell lines expressing receptors for each coronavirus (Figure S3 A-F). Surprisingly, we did not observe any significant differences in the capability of all tested coronaviruses to replicate in cells lacking IRE1α (Figure 6C-F). These results suggest IRE1α is not essential for coronavirus replication. Since SARS-CoV-2 does not lead to IRE1α-mediated XBP1 splicing, we also tested replication of SARS-CoV-2 and OC43 in XBP1 KO cells (Figure 6C&D and S3G). Consistently, there was no detectable effect of XBP1 KO on SARS-CoV-2 or OC43 replication in A549-ACE2. Together, these results demonstrate that none of the coronaviruses tested require the activation IRE1α/XBP1 pathway for replication.

DISCUSSION

SARS-CoV-2 is the third in a series of betacoronavirus family members that initiate infection the upper respiratory tract but have the potential to cause life-threatening pneumonia as a result of infection and inflammation of the lower respiratory tract. The aberrant pulmonary response to severe infection with CoV is associated with marked dysfunction in the distal lung (alveolar) epithelium, which includes disruption of barrier function, dysregulated immune responses, transcriptomic reprogramming to a transitional cell state, and senescence (30, 31). To better understand the host epithelial response to CoV, we systematically compared the activation of the IRE1α/XBP1 pathway of the UPR during infection with four betacoronaviruses in two lung-derived cells lines, A549 and Calu-3, and iPSC-derived AT2 cells. We employed three human viruses, each from a different betacoronavirus lineage, HCoV-OC43 (embeco), SARS-CoV-2 (sarbeco) and MERS-CoV (merbeco), and also included the model murine coronavius MHV, an embecovirus. We found a striking difference between the response of SARS-CoV-2 and the other three viruses. HCoV-OC43, MHV and MERS-CoV all activated the canonical IRE1α/XBP1 pathway in both A549 and Calu-3 cells as evidenced by phosphorylation of IRE1α (Figure 2), XBP1 splicing (Figure 3&4) and induction of DNAJB9 (Figure 3), a target of XBP1s. Additionally, MERS-CoV was observed to also induce IRE1α/XBP1 activation in iAT2 cells (Figure 5). In contrast, while SARS-CoV-2 also promoted autophosphorylation of IRE1α, there was no evidence of XBP1s, indicating that the pathway was only partially activated and suggesting that the IRE1α kinase activity was active while the RNase activity was not. The differential splicing of XBP1 during SARS-CoV-2 and MERS-CoV infection was also observed in iPSC-derived AT2 cells, confirming the results in a more physiologically relevant system (Figure 5). The difference among these viruses is suprising as the viral replicase encoded proteins nsp3, 4 and 6 required for formation of replication factories in the DMV as well as three membrane associated glycoproteins

that flood the ER would be expected to induce similar stress on the ER and lead to UPR activation. Indeed, our data suggest that that SARS-CoV-2 actively prevents XBP1 splicing (Figure 6A,B &G). Consistent with this idea, a recombinant SARS-CoV lacking the E protein (rSARS-CoV-ΔE) was reported to induce more XBP1 splicing as well as induction of UPR genes compared to parental wild type virus (32).

Multiple coronavirus family members, including HCoV-OC43 (25), MHV (20), IBV (33), have been reported to activate IRE1α [reviewed in (6)]. In the few instances where its functional role in coronavirus infection has been tested, IRE1α has been reported to be critical for viral replication and cytotoxicity. For example, knockdown and overexpression experiments demonstrated that IRE1α protects infected cells from IBV-induced apoptosis (33). In addition, over-expression of spike proteins from MHV, SARS-CoV, SARS-CoV-2, and HKU1 all induce ER stress and UPR activation in cultured cells (34). Other SARS-CoV-encoded accessory proteins, including proteins 3a, 6 and 8ab, as well as SARS-CoV-2 Orf8 protein (22, 35), have also been reported to induce ER stress when over-expressed in cells (36-38). However, caution must be taken in interpreting effects of overexpressed proteins and a role for these in infection has not been confirmed.

Most current evidence suggests that virus-induced hyperactivation of IRE1α/XBP1 is critical to massively increase ER capacity in host cells in order to accommodate the inordinate stress of increased viral protein production. Indeed, inhibition of IRE1α has been reported to be detrimental to influenza A virus replication (39). Of the three arms of the UPR, IRE1α is the most important for signaling ER expansion. IRE1α-mediated XBP1 splicing results in production of the Xbp1s transcription factor whose target genes include many involved in lipid biogenesis and vesicular trafficking (40). Forced expression of Xbp1s is sufficient to induce synthesis of phosphatidylcholine, the primary phospholipid of the ER membrane, and massively increase the

surface area and volume of the rough ER (41). As such, activation of IRE1α/Xbp1s causes the ER to expand in size and function. Moreover, given its extensive communication with other key signaling pathways (mitogen-activated protein kinase pathways, inflammatory responses, apoptosis, autophagy and innate immunity), the UPR may coordinate multiple anti-viral responses and constitute a critical coronavirus-host interaction(6). In summary, hyperactivation of the UPR, and its IRE1α-/XBP1 branch in particular, is often considered a general feature of infection by coronaviruses.

To investigate the importance of IRE1α for CoV replication, we evaluated replication of each of the betacoronaviruses in IRE1α KO A549 cells. In contrast to influenza, all of the betacoronaviruses examined were able to replicate efficiently in the absence of IRE1α signaling. This raises interesting possibilities for the role of IRE1α during CoV infection. As previously stated, IRE1α can produce both cytoprotective (through XBP1s) and destructive responses (via RIDD and JNK/p38 signaling) depending on the extent of the encountered stress. It seems likely that CoV infection would induce extensive and prolonged ER stress, which may push IRE1α beyond the initial pro-recovery responses and towards a pro-apoptitic response. Indeed, our data reveal that, at least with MERS-CoV and SARS-CoV-2 infection, IRE1α phosphorylation is readily detectable by 24hpi and remains steady throughout the course of infection (Figure S1A&B). Additionally, unlike what has been observed with chemically-induced ER stress (26, 42), IRE1α phosphorylation does not appear to attenuate at any point during CoV infection, again suggesting a hyperactive and destructive outcome. As stated above, destruction of cells, in particular AT2 cells in the lung, may contribute to pathogenesis during CoV infection. However, SARS-CoV-2 appears to limit the downstream consequences of IRE1α activation, most notably XBP1 splicing via its RNase activity and thus may be protected from this destructive phenotype. MERS-CoV may induce apoptosis redundantly in the UPR, as it has been reported that MERS-CoV induces and benefits from apoptisis mediated by the PERK arm of the UPR (21, 43). Overall, despite the

lack of apparent virus replication defects with IRE1α deficinecy, further characterization of the repertoire of betacoronavirus induced IRE1α signaling is warranted, including contributions to cytokine production, apoptosis, and pro-inflammatory responses. While we have initially investigated this pathway from the perspective of the impact on virus replication, future studies will examine effects of IRE1α activation on the host, including inflammation and cell death through the JNK and p38 MAPK signaling scaffolded by IRE1α (16) and/or RIDD, a consequence of prolonged IRE1α activation (11, 44). These responses could be particularly important in AT2 cells, which must rely on the UPR to maintain proteostasis in the face of the challenge from the biosynthesis and secretion of surfactant proteins (45). Dysregulation of these responses by CoV infection could promote AT2 cell reprogramming, epithelial apotosis, alteration of surfactant components in alveoli, and the rampant inflammation associated with severe CoV infection (46-48). Finally, the UPR response is complex and made up of the PERK and ATF6 pathways in addition to IRE1α, and signals from all three of these pathways almost certainly integrate into the final outcome of an infected cell.

Considering the differences we have observed between betacoronaviruses with IRE1α activation and signaling, it is striking that MERS-CoV and SARS-CoV-2 are reciprocal in which they activate and antagonize. To that point, we recently reported that SARS-CoV-2 activates double-stranded RNA induced host antiviral pathways (oligonucledotide synthetase/ribonuclease L and protein kinase R and to some extent interferon signaling), while MERS-CoV nearly completely supresses these responses (3). Thus, we suggest that to optimize replication, CoVs must likely strike a balance in which cellular responses they antagonize, tolerate, or benefit from. Future studies should examine the synergy between innate immune responses and the UPR during CoV infection, and how perturbations on one side may change viral replicative capacity, tropism, and spread. Understanding how signals from each one of these pathways are integrated into viral

replication and cell fate decisions during CoV infection may illuminate new therapeutic strategies for combating emerging betacoronaviruses.

MATERIALS AND METHODS

Cell lines

Human A549 cells (ATCC CCL-185) and its derivatives were cultured in RPMI 1640 (Gibco catalog no. 11875) supplemented with 10% FBS, 100 U/ml of penicillin, and 100 µg/ml streptomycin (Gibco catalog no. 15140). African green monkey kidney Vero cells (E6) (ATCC CRL-1586) and VeroCCL81 cells (ATCC CCL-81) were cultured in Dulbecco's modified Eagle's medium (DMEM; Gibco catalog no. 11965), supplemented with 10% fetal bovine serum (FBS), 100 U/ml of penicillin, 100 µg/ml streptomycin, 50 µg/ml gentamicin (Gibco catalog no. 15750), 1mM sodium pyruvate (Gibco catalog no. 11360), and 10mM HEPES (Gibco catalog no. 15630). Human HEK 293T cells (ATCC) were cultured in DMEM supplemented with 10% FBS. Human Calu-3 cells (ATCC HTB-55) were cultured in MEM supplemented with 20% FBS without antibiotics. Mouse L2 cells(49) were grown in DMEM supplemented with 10% FBS, 100U/mL of penicillin, 100µg/mL streptomycin, 10nM HEPES, 2mM L-glutamine (Gibco catalog no. 25030081), and 2.5µg/mL Amphotericin B (Gibco catalog no. 15290).

A549-DPP4 (4), A549-ACE2 (3) and A549-MHVR (4) cells were generated as described previously. A549-ACE2 cells, used in Figure 3I&J, Figure 4, Figure 6, and Figure S3 were a kind gift of Benjamin TenOever, Mt Sinai Icahn School of Medicine. CRISPR-Cas9 knockout cell lines were generated using lentiviruses. Lentivirus stocks were generated by using lentiCRISPR v2 (Addgene) with single guide RNA (sgRNA) targeting IRE1α sequences: Version1 (V1):CGGTCACTCACCCCGAGGCC, version (V2): TTCAGGAAGCGTCACTGTGC, version (V3): CGGTCACTCACCCCGAGGCC; or XBP1 sequence: TCGAGCCTTCTTTCGATCTC. The

infected A549-ACE2 cells were polyclonally selected and maintained by culture in media supplemented with 4 µg/mL puromycin for 1 week.

iPSC (SPC2 iPSC line, clone SPC2-ST-B2, Boston University) derived alveolar epithelial type 2 cells (iAT2) were grown and infected as previously described (3). In brief, cells were differentiated and maintained as alveolospheres embedded in 3D Matrigel in CK+DCI media, as previously described (50). For generation of 2D alveolar cells for viral infection, alveolospheres were dispersed into single cells, then plated on pre-coated 1/30 Matrigel plates at a cell density of 125,000 cells/cm2 using CK+DCI media with ROCK inhibitor for the first 48h and then the medium was changed to CK+DCI media at day 3 and infected with either mock infected or infected with MERS-CoV or SARS-CoV-2 at a MOI of 5.

Viruses

SARS-CoV-2 (USA-WA1/2020 isolate) was obtained from BEI Resources, NIAID, NIH or provided by Natalia Thornburg, World Reference Center for Emerging Viruses and Arboviruses (Galveston, Texas), and propagated in VeroE6-TMPRSS2 cells. The genome RNA was sequenced and found to be identical to GenBank: MN985325.1. Recombinant MERS-CoV was described previously (1) and propagated in VeroCCL81 cells. All SARS-CoV-2 infections were performed in biosafety level 3 laboratories at the Howard Taylor Ricketts Laboratory (HTRL) at Argonne National Laboratory (Lemont, IL) or the University of Pennsylvania, where all MERS-CoV infections were performed under BSL-3 conditions, using appropriate and approved personal protective equipment and protocols. OC43 was obtained from ATCC (VR-1558) grown and titrated on A549-mRuby cells as desrcibed (51) or VeroE6 cells at 33 degrees Celsius. MHV-A59 was obtained from Thomas Gallagher, Loyola's Stritch School of Medicine (52) and propagated on A549-MHVR cells or on murine 17CL-1 cells.

Viral growth kinetics and titration

SARS-CoV-2 and MERS-CoV infections and plaque assays were performed as previously described (1, 5). In brief, A549 cells were seeded at $3x10^5$ cells per well in a 12-well plate for infections. Calu-3 cells were seeded similarly onto rat tail collagen type I coated plates (Corning #356500). Cells were washed once with PBS before infecting with virus diluted in serum free media – RPMI for A549 cells or DMEM for Calu-3 cells. Virus was absorbed for 1 hour (A549 cells) or 2 hours (Calu-3 cells) at 37 degrees Celsius before the cells were washed 3 times with PBS and the media replaced with 2% FBS RPMI (A549 cells) or 4% FBS DMEM (Calu-3 cells). At the indicated timepoints, 200µL of media was collected to quantify released virus by plaque assay, and stored at -80 degrees Celsius. Infections for MHV growth curves were performed similarly in BSL-2 conditions. For OC43 infections, similar infection conditions and media were used, however virus was absorbed and the infections incubated at 33 degrees Celsius rather than 37 degrees.

Plaque assays were performed using VeroE6 cells for SARS-CoV-2 and OC43; VeroCCL81 cells for MERS-CoV; and L2 cells for MHV. SARS-CoV-2 and MERS-CoV plaque assays were performed in 12-well plates at 37 degrees Celsius. OC43 and MHV plaque assays were performed in 6-well plates at 33 degrees Celsius and 37 degrees Celsius, respectively. In all cases, virus was absorbed onto cells for one hour at the indicated temperatures before overlay was added. For SARS-CoV-2, MERS-CoV, and OC43 plaque assays, a liquid overlay was used (DMEM with 2% FBS, 1x sodium pyruvate, and 0.1% agarose). A solid overlay was used for MHV plaque assays (DMEM plus 2% FBS, 1x HEPES, 1x glutamine, 1x Fungizone, and 0.7% agarose). Cell monolayers were fixed with 4% paraformaldehyde and stained with 1% crystal violet after the following incubation times: SARS-CoV-2 and MERS-CoV, 3 days; OC43, 5 days; MHV, 2 days. All plaque assays were performed in biological triplicate and technical duplicate.

Pharmacologic agents

KIRA8 was purchased at >98% purity from Chemveda Life Sciences India Pvt. Ltd. For use in tissue culture, KIRA8 stock solution was prepared by dissolving in DMSO. Tunicamycin(cat. #T7765) and thapsigargin (cat. #T9033) were purchased at >98% purity from Sigma. For use in tissue culture, Tunicamycin stock solution was prepared by dissolving in DMSO.

Immunoblotting

Cells were washed once with ice-cold PBS and lysates harvested at the indicated times post infection with lysis buffer (1% NP-40, 2mM EDTA, 10% glycerol, 150mM NaCl, 50mM Tris HCl, pH 8.0) supplemented with protease inhibitors (Roche complete mini EDTA-free protease inhibitor) and phosphatase inhibitors (Roche PhosStop easy pack). After 5 minutes, lysates were incubated on ice for 20 minutes, centrifuged for 20 minutes at 4°C and supernatants mixed 3:1 with 4x Laemmli sample buffer (Bio-rad 1610747). Samples were heated at 95°C for 5 minutes, then separated on SDS-PAGE, and transferred to PVDF membranes. Blots were blocked with 5% nonfat milk or 5% BSA and probed with antibodies (table below) diluted in the same block buffer. Primary antibodies were incubated overnight at 4°C or for 1 hour at room temperature. All secondary antibody incubation steps were done for 1 hour at room temperature. Blots were visualized using Thermo Scientific SuperSignal chemiluminescent substrates (Cat #: 34095 or 34080).

Primary Antibody	**Antibody species**	**Blocking buffer**	**Dilution**	**Catalog number**
Phospho-IRE1α	rabbit	5% BSA	1:1000	Abcam (EPR5253)

IRE1α (14C10)	rabbit	5% milk/TBST	1:1000	Cell Signaling Technology 3294S
XBP1	mouse	5% milk/TBST	1:1000	Biolegend 9D11A43
GAPDH (14C10)	rabbit	5% milk/TBST	1:2000	Cell Signaling Technology 2118S
SARS-CoV-2 N	rabbit	5% milk/TBST	1:2000	GTX135357 (Gentex)
MERS-CoV N	mouse	5% milk/TBST	1:2000	40068-MM10 (Sino Biological)
OC43 N	rabbit	5% milk/TBST	1:2000	40643-T62 (Sino Biological)

RNA sequencing

Lung alveolar A549 cells expressing the MERS-CoV receptor DPP4 (4) were cultured in 10% FBS RPMI media. At 70% cell confluence, cells were washed once with PBS before being mock infected or infected with MERS-CoV (EMC/2012) at MOI = 1. Virus was absorbed for 1 hour at 37 degrees Celsius in serum-free RPMI media. After one hour, virus was removed, cells washed three times with PBS, and 2% FBS RPMI was added. The cells were incubated for another 24 hours or 36 hours, then washed once with PBS and lysed using RLT Plus lysis buffer before genomic DNA removal and total RNA extraction using the Qiagen RNeasy Plus Mini Kit (Qiagen 74134). Three independent biological replicates were performed per experimental condition. RNA sample quality check, library construction, and sequencing were performed by GeneWiz following standard protocols. All samples were sequenced by an Illumina HiSeq sequencer to generate

paired-end 150bp reads. Read quality was assessed using FastQC v0.11.2 as described by Andrews, S. (2010). “FastQC: A Quality Control Tool for High Throughput Sequence Data.”: *http://www.bioinformatics.babraham.ac.uk/projects/fastqc/*. Raw sequencing reads from each sample were quality and adapter trimmed using BBDuk 38.73 as described by Bushnell, B at "BBTools software package.": *http://sourceforge. net/projects/bbmap* 578 (2014): 579. The reads were mapped to the human genome (hg38 with Ensembl V98 annotation) using RNA STAR 2.7.1a(53). The resulting BAM files were counted by featureCounts 1.6.4 to count the number of reads for each gene(54). Differential expression between mock, 24hpi, and 36hpi experimental conditions were analyzed using the raw gene counts files by DESeq2 1.22.1(55). A PCA plot of RNA-seq samples and a normalized gene expression matrix were also generated by DESeq2.

Host pathway activity analysis of viruses

RNA-seq data from GSE147507(27), GSE168797, GSE144882 (24) and above were used to compare effects of different viruses on host ER stress response. Specifically, Ingenuity Pathway Analysis (IPA) (https://www.qiagenbioinformatics.com/products/ingenuitypathway-analysis) was used to predict activities of related canonical pathways based on host gene expression changes following viral infection. Activation z-scores for every virus and canonical pathway combination were plotted as a heatmap using Morpheus (https://software.broadinstitute.org/morpheus). IPA used the following q-value cutoffs for each dataset to perform the canonical pathway cross comparison: Calu3 SARS-CoV-2 MOI 2 24hr $q<0.05$, NHBE SARS-CoV-2 MOI 2 24hr $q<0.1$, A549-ACE2 SARS-CoV-2 MOI 0.2 24hr $q<0.1$, A549-ACE2 SARS-CoV-2 MOI 2 24hr $q<0.05$, A549-ACE2 SARS-CoV-2 MOI 3 24hr $q<0.01$, A549-DPP4 MERS-CoV MOI 1 24hr $q<0.1$, A549-DPP4 MERS-CoV MOI 1 36hr $q<0.01$, BMDM MHV-A59 MOI 1 12hr $q<0.1$ and over 1-fold up or down-regulated. These cutoffs were implemented due to the limitations set by the IPA software.

Statistical analysis

All statistical analyses and plotting of data were performed using GraphPad Prism software. RT-qPCR data were analyzed by Student *t* test. Plaque assay data were analyzed by two-way ANOVA with multiple comparisons correction. Displayed significance is determined by p-value (P), where * = P < 0.05; ** = P < 0.01; *** = P < 0.001; **** = P < 0.0001; ns = not significant.

Quantification of XBP1 alternative splicing using RNA-seq data

BAM files produced by RNA STAR were analyzed in Integrative Genomics Viewer 2.9.4 to count the number of XBP1 reads containing the alternative splicing (56). The total number of XBP1 reads were counted by featureCounts. The percentage of XBP1 alternative splicing for each sample was determined by dividing the number of alternatively spliced reads by the number of total XBP1 reads (spliced plus unspliced). XBP1 alternatively splicing of MERS was analyzed using the RNA-seq data (see above). The same analysis was performed on SARS-CoV-2 using the RNA-seq data published in GSE168797(57).

Quantitative PCR (RT-qPCR)

Cells were lysed with RLT Plus buffer and total RNA was extracted using the RNeasy Plus Mini Kit (Qiagen). RNA was reverse transcribed into cDNA with a High Capacity cDNA Reverse Transcriptase Kit (Applied Biosystems). cDNA samples were diluted in molecular biology grade water and amplified using specific RT-qPCR primers (see Table below). RT-qPCR experiments were performed on a Roche LightCycler 96 Instrument. SYBR Green Supermix was from Bio-Rad. Host gene expression displayed as fold change over mock-infected samples was generated

by first normalizing cycle threshold (C_T) values to 18S rRNA to generate ΔDC_T values ($\Delta C_T = C_T$ gene of interest - C_T 18S rRNA). Next, Δ (DC_T) values were determined by subtracting the mock-infected DC_T values from the virus infected samples. Technical triplicates were averaged and means displayed using the equation $2^{-\Delta(\Delta CT)}$.

Primer sequences lists:

	Forward primer (5' to 3')	Reverse primer (5' to 3')
XBP1s	GCTGAGTCCGCAGCAGGT	CTGGGTCCAAGTTGTCCAGAAT
XBP1 total	TGAAAACAGAGTAGCAGCTCAGA	CCCAAGCGCTGTCTTAACTC
RPL13A	CTCAAGGTGTTTGACGGCATCC	TACTTCCAGCCAACCTCGTGAG
18S rRNA	TTCGATGGTAGTCGCTGTGC	CTGCTGCCTTCCTTGAATGTGGTA
SARS-CoV-2 genome (nsp12/RdRp)	GGTAACTGGTATGATTTCG	CTGGTCAAGGTTAATATAGG
MERS-CoV genome (nsp7)	GCACATCTGTGGTTCTCCTCTCT	AAGCCCAGGCCCTACTATTAGC
DNAJB9	AGTCGGAGGGTGCAGGATATT	TTGATTTGGCGCTCTGATGC

<u>XBP1 splicing assay by RT-qPCR</u>

RT-qPCR was used to quantify the relative expression of the spliced version of XBP1 (XBP1s) by using specific pairs of primers for human alternatively spliced XBP1 and total XBP1 (primer

sequences are described above) as previously described (58). The relative percentage of alternative splicing of XBP1 (%XBP1s) was indicated by calculating the ratio of signals between XBP1s and total XBP1.

Acknowledgments. We thank Alejandra Fausto for help with OC43 propagation and titration and Dr. Rachel Truitt and the Penn iPSC Core for preparation of the iAT2 cells. We thank the members of SARS-CoV-2 host response team in Chicago for stimulating discussions and support: particularly Julian Solway, Rick Morimoto, Nissim Hay, Raymond Roos, and Dominique Missiakas. This work was supported by National Institutes of Health grant R01-AI140442 and supplement for SARS-CoV-2 (S.R.W), R01CA219815 (S.A.O.), R01EY027810 (S.A.O.), U01DK127786 (S.A.O.), R01 GM121735 (M.R.R.); Department of Veterans Affairs Merit Review 2I01BX005411 (M.F.B.&S.R.W.); Penn Center for Research on Coronaviruses and Other Emerging Pathogens (S.R.W). BIG Vision grant from the University of Chicago (M.R.R.). DMR was supported in part by T32 AI055400.

Disclosures

S.R.W. is on the Scientific Advisory Boards of Immunome, Inc and Ocugen, Inc.
S.A.O. is a cofounder and consultant at OptiKira., L.L.C. (Cleveland, OH)

REFERENCES:

1. A. R. Fehr, S. Perlman, Coronaviruses: an overview of their replication and pathogenesis. *Methods Mol Biol* **1282**, 1-23 (2015).
2. A. E. Gorbalenya, L. Enjuanes, J. Ziebuhr, E. J. Snijder, Nidovirales: evolving the largest RNA virus genome. *Virus Res* **117**, 17-37 (2006).
3. Y. Li *et al.*, SARS-CoV-2 induces double-stranded RNA-mediated innate immune responses in respiratory epithelial-derived cells and cardiomyocytes. *Proc Natl Acad Sci U S A* **118** (2021).

4. C. E. Comar *et al.*, Antagonism of dsRNA-Induced Innate Immune Pathways by NS4a and NS4b Accessory Proteins during MERS Coronavirus Infection. *mBio* **10** (2019).
5. L. Zhao *et al.*, Antagonism of the interferon-induced OAS-RNase L pathway by murine coronavirus ns2 protein is required for virus replication and liver pathology. *Cell Host Microbe* **11**, 607-616 (2012).
6. T. S. Fung, M. Huang, D. X. Liu, Coronavirus-induced ER stress response and its involvement in regulation of coronavirus-host interactions. *Virus Res* **194**, 110-123 (2014).
7. T. S. Fung, D. X. Liu, Coronavirus infection, ER stress, apoptosis and innate immunity. *Front Microbiol* **5**, 296 (2014).
8. K. J. Travers *et al.*, Functional and genomic analyses reveal an essential coordination between the unfolded protein response and ER-associated degradation. *CELL* **101**, 249-258 (2000).
9. K. Zhang, R. J. Kaufman, The unfolded protein response: a stress signaling pathway critical for health and disease. *Neurology* **66**, S102-109 (2006).
10. H. P. Harding, M. Calfon, F. Urano, I. Novoa, D. Ron, Transcriptional and translational control in the Mammalian unfolded protein response. *Annu Rev Cell Dev Biol* **18**, 575-599 (2002).
11. D. Han *et al.*, IRE1alpha kinase activation modes control alternate endoribonuclease outputs to determine divergent cell fates. *Cell* **138**, 562-575 (2009).
12. R. Ghosh *et al.*, Allosteric Inhibition of the IRE1alpha RNase Preserves Cell Viability and Function during Endoplasmic Reticulum Stress. *Cell* **158**, 534-548 (2014).
13. M. Calfon *et al.*, IRE1 couples endoplasmic reticulum load to secretory capacity by processing the XBP-1 mRNA. *Nature* **415**, 92-96 (2002).
14. H. Yoshida, T. Matsui, A. Yamamoto, T. Okada, K. Mori, XBP1 mRNA is induced by ATF6 and spliced by IRE1 in response to ER stress to produce a highly active transcription factor. *Cell* **107**, 881-891 (2001).
15. A. H. Lee, N. N. Iwakoshi, L. H. Glimcher, XBP-1 regulates a subset of endoplasmic reticulum resident chaperone genes in the unfolded protein response. *Mol Cell Biol* **23**, 7448-7459 (2003).
16. C. Hetz, The unfolded protein response: controlling cell fate decisions under ER stress and beyond. *Nat Rev Mol Cell Biol* **13**, 89-102 (2012).
17. J. P. Upton *et al.*, IRE1alpha cleaves select microRNAs during ER stress to derepress translation of proapoptotic Caspase-2. *Science* **338**, 818-822 (2012).

18. A. Chakrabarti, B. K. Jha, R. H. Silverman, New insights into the role of RNase L in innate immunity. *J Interferon Cytokine Res* **31**, 49-57 (2011).
19. B. He, Viruses, endoplasmic reticulum stress, and interferon responses. *Cell Death Differ* **13**, 393-403 (2006).
20. J. Bechill, Z. Chen, J. W. Brewer, S. C. Baker, Coronavirus infection modulates the unfolded protein response and mediates sustained translational repression. *J Virol* **82**, 4492-4501 (2008).
21. A. C. Sims *et al.*, Unfolded Protein Response Inhibition Reduces Middle East Respiratory Syndrome Coronavirus-Induced Acute Lung Injury. *mBio* **12**, e0157221 (2021).
22. L. Echavarria-Consuegra *et al.*, Manipulation of the unfolded protein response: A pharmacological strategy against coronavirus infection. *PLoS Pathog* **17**, e1009644 (2021).
23. E. B. Prestes, J. C. P. Bruno, L. H. Travassos, L. A. M. Carneiro, The Unfolded Protein Response and Autophagy on the Crossroads of Coronaviruses Infections. *Front Cell Infect Microbiol* **11**, 668034 (2021).
24. A. Volk *et al.*, Coronavirus Endoribonuclease and Deubiquitinating Interferon Antagonists Differentially Modulate the Host Response during Replication in Macrophages. *J Virol* **94** (2020).
25. D. J. Favreau, M. Desforges, J. R. St-Jean, P. J. Talbot, A human coronavirus OC43 variant harboring persistence-associated mutations in the S glycoprotein differentially induces the unfolded protein response in human neurons as compared to wild-type virus. *Virology* **395**, 255-267 (2009).
26. T. K. Chang *et al.*, Coordination between Two Branches of the Unfolded Protein Response Determines Apoptotic Cell Fate. *Mol Cell* **71**, 629-636 e625 (2018).
27. D. Blanco-Melo *et al.*, Imbalanced Host Response to SARS-CoV-2 Drives Development of COVID-19. *Cell* **181**, 1036-1045 e1039 (2020).
28. Y. M. Arabi *et al.*, Middle East Respiratory Syndrome. *N Engl J Med* **376**, 584-594 (2017).
29. J. P. Bridges, E. K. Vladar, H. Huang, R. J. Mason, Respiratory epithelial cell responses to SARS-CoV-2 in COVID-19. *Thorax* 10.1136/thoraxjnl-2021-217561 (2021).
30. F. D'Agnillo *et al.*, Lung epithelial and endothelial damage, loss of tissue repair, inhibition of fibrinolysis, and cellular senescence in fatal COVID-19. *Sci Transl Med* **13**, eabj7790 (2021).
31. J. C. Melms *et al.*, A molecular single-cell lung atlas of lethal COVID-19. *Nature* **595**, 114-119 (2021).

32. M. L. DeDiego *et al.*, Severe acute respiratory syndrome coronavirus envelope protein regulates cell stress response and apoptosis. *PLoS Pathog* **7**, e1002315 (2011).
33. T. S. Fung, Y. Liao, D. X. Liu, The endoplasmic reticulum stress sensor IRE1alpha protects cells from apoptosis induced by the coronavirus infectious bronchitis virus. *J Virol* **88**, 12752-12764 (2014).
34. C. P. Chan *et al.*, Modulation of the unfolded protein response by the severe acute respiratory syndrome coronavirus spike protein. *J Virol* **80**, 9279-9287 (2006).
35. F. Rashid, E. E. Dzakah, H. Wang, S. Tang, The ORF8 protein of SARS-CoV-2 induced endoplasmic reticulum stress and mediated immune evasion by antagonizing production of interferon beta. *Virus Res* **296**, 198350 (2021).
36. R. Minakshi *et al.*, The SARS Coronavirus 3a protein causes endoplasmic reticulum stress and induces ligand-independent downregulation of the type 1 interferon receptor. *PLoS One* **4**, e8342 (2009).
37. S. C. Sung, C. Y. Chao, K. S. Jeng, J. Y. Yang, M. M. Lai, The 8ab protein of SARS-CoV is a luminal ER membrane-associated protein and induces the activation of ATF6. *Virology* **387**, 402-413 (2009).
38. Z. Ye, C. K. Wong, P. Li, Y. Xie, A SARS-CoV protein, ORF-6, induces caspase-3 mediated, ER stress and JNK-dependent apoptosis. *Biochim Biophys Acta* **1780**, 1383-1387 (2008).
39. I. H. Hassan *et al.*, Influenza A viral replication is blocked by inhibition of the inositol-requiring enzyme 1 (IRE1) stress pathway. *J Biol Chem* **287**, 4679-4689 (2012).
40. L. H. Glimcher, XBP1: the last two decades. *Ann Rheum Dis* **69 Suppl 1**, i67-71 (2010).
41. R. Sriburi, S. Jackowski, K. Mori, J. W. Brewer, XBP1: a link between the unfolded protein response, lipid biosynthesis, and biogenesis of the endoplasmic reticulum. *J Cell Biol* **167**, 35-41 (2004).
42. H. Li, A. V. Korennykh, S. L. Behrman, P. Walter, Mammalian endoplasmic reticulum stress sensor IRE1 signals by dynamic clustering. *Proc Natl Acad Sci U S A* **107**, 16113-16118 (2010).
43. H. Chu *et al.*, Targeting highly pathogenic coronavirus-induced apoptosis reduces viral pathogenesis and disease severity. *Sci Adv* **7** (2021).
44. J. Hollien, J. S. Weissman, Decay of endoplasmic reticulum-localized mRNAs during the unfolded protein response. *Science* **313**, 104-107 (2006).
45. J. Katzen, M. F. Beers, Contributions of alveolar epithelial cell quality control to pulmonary fibrosis. *J Clin Invest* **130**, 5088-5099 (2020).

46. Y. Yamamoto, A. Ohtori, In vitro study of aldose reductase inhibitor concentrations in the lens and inhibitory effect on sugar alcohol accumulation. *Curr Eye Res* **9**, 421-428 (1990).
47. J. A. Maguire, S. Mulugeta, M. F. Beers, Multiple ways to die: delineation of the unfolded protein response and apoptosis induced by Surfactant Protein C BRICHOS mutants. *Int J Biochem Cell Biol* **44**, 101-112 (2012).
48. J. Katzen *et al.*, An SFTPC BRICHOS mutant links epithelial ER stress and spontaneous lung fibrosis. *JCI Insight* **4** (2019).
49. J. L. Gombold, S. T. Hingley, S. R. Weiss, Fusion-defective mutants of mouse hepatitis virus A59 contain a mutation in the spike protein cleavage signal. *J Virol* **67**, 4504-4512 (1993).
50. A. Jacob *et al.*, Derivation of self-renewing lung alveolar epithelial type II cells from human pluripotent stem cells. *Nat Protoc* **14**, 3303-3332 (2019).
51. N. Drayman *et al.*, Masitinib is a broad coronavirus 3CL inhibitor that blocks replication of SARS-CoV-2. *Science* **373**, 931-936 (2021).
52. A. Shulla, T. Gallagher, Role of spike protein endodomains in regulating coronavirus entry. *J Biol Chem* **284**, 32725-32734 (2009).
53. A. Dobin *et al.*, STAR: ultrafast universal RNA-seq aligner. *Bioinformatics* **29**, 15-21 (2013).
54. Y. Liao, G. K. Smyth, W. Shi, featureCounts: an efficient general purpose program for assigning sequence reads to genomic features. *Bioinformatics* **30**, 923-930 (2014).
55. M. I. Love, W. Huber, S. Anders, Moderated estimation of fold change and dispersion for RNA-seq data with DESeq2. *Genome Biol* **15**, 550 (2014).
56. J. T. Robinson *et al.*, Integrative genomics viewer. *Nat Biotechnol* **29**, 24-26 (2011).
57. L. C. Nguyen *et al.*, Cannabidiol Inhibits SARS-CoV-2 Replication and Promotes the Host Innate Immune Response. *bioRxiv* 10.1101/2021.03.10.432967 (2021).
58. S. B. Yoon *et al.*, Real-time PCR quantification of spliced X-box binding protein 1 (XBP1) using a universal primer method. *PLoS One* **14**, e0219978 (2019).

Figure legends

Figure 1. Coronavirus family.

Phylogenetic tree of betacoronaviruses and their lineages. Viruses examined in this study are show in red font.

Figure 2. Induction of IRE1α phosphorylation following coronavirus infection.

A549 cells expressing the indicated viral receptors were mock infected or infected with the indicated viruses, protein was harvested at the indicated time and analyzed by immunoblotting with the indicated antibodies. (A,C,F) Cells infected with OC43, MOI=4 (A) or MHV, MOI=0.1 (C) or SARS-CoV-2 at MOI=3 (F) were pre-treated 2 hours prior to infection with KIRA8. (B,D,E) Cells were infected with OC43 at MOI=1 (B), MERS-CoV, MOI=5 (D), or SARS-CoV-2, MOI=5 (E) or treated with DMSO, thapsigargin (Tg, 1μM) for 1 hour or tunicamycin (TM, 1μg/ mL) for 8 hours. (G) Calu-3 cells were mock infected, or infected with MERS-CoV, or SARS-CoV-2 (MOI=5). Protein was harvested at 24 or 48 hours post infection and analyzed by immunoblotting with indicated antibodies. Data shown are from one representative experiment of at least two independent experiments.

Figure 3. IRE1α-mediated XBP1 splicing occurs following infection with OC43 or MERS but not SARS-CoV-2.

A549 cells were mock infected or infected (in triplicate) with OC43, MOI=1 (A, E), MERS-CoV, MOI=5 (B, F), SARS-CoV-2, MOI=5 (C, G) or with Tm (1μg/ mL) for 8 hours and total RNA harvested at indicated time points. (A-D) Relative %XBP1s, XBP1s, total XBP1 and DNAJB9 mRNA expression were quantified by RT-qPCR. C_T values were normalized to 18S rRNA and expressed as fold-change over mock displayed as $2^{-\Delta(\Delta Ct)}$. Technical replicates were averaged, the means for each replicate displayed, ±SD (error bars). (D) Calu-3 cells were mock infected or

infected with MERS-CoV or SARS-CoV-2 (MOI=5) and total RNA harvested at indicated time points. Relative %XBP1s, XBP1s, total XBP1 and DNAJB9 mRNA expression were quantified by RT-qPCR, calculated, and displayed as described above. Values are means ± SD (error bars). Statistical significance were determined using two-tailed, paired Student *t*-test. Displayed significance (infected relative to mock) is determined by p-value (P), where * = P < 0.05; ** = P < 0.01; *** = P < 0.001; **** = P < 0.0001; ns = not significant. (E-H) RNA was harvested from A549 cells mock infected or infected with OC43, MOI=1 (E), MERS-CoV, MOI=5 (F), SARS-CoV-2, MOI=5 (G), or Calu-3 cells infected with MERS-CoV and SARS-CoV-2, MOI=5 (H) or treated with tunicamycin (Tm, 1μg/ mL) for 8 hour, or thapsigargin (Tg, 1μM) for 1 hour or DMSO. RT-PCR was performed using primers crossing the XBP1 splicing site. The product was run an on an agarose gel to visualize XBP1 splicing. (I-J) Lysates from A549-ACE2 cells mock infected, or Tm (500 ng/mL) for 6 hours or infected with OC43 (MOI=4) or SARS-CoV-2 (MOI=3), treated with or without KIRA8, were harvested at indicated time points as Figure 2A,C&F and immunoblotted for XBP1s protein. Data shown are from one representative experiment from at least three independent experiments.

Figure 4. Unlike other coronaviruses, SARS-CoV-2 infection does not lead to robust UPR activation.

(A) Heatmap of predicted pathway status based on Ingenuity Pathway Analysis (IPA) of activation z-scores for each pathway from RNA-sequencing data from indicated cells infected with SARS-CoV-2, MERS-CoV or MHV under specified conditions. Red: pathway predicted to be activated. Blue: pathway predicted to be inhibited. White: pathway predicted to be unchanged. Gray: no prediction due to lack of significance. (B&C) Quantification of XBP1 splicing by analyzing RNA-Seq data from A549-DPP4 and A549-ACE2 cells mock-infected or infected with MERS-CoV or SARS-CoV-2, respectively, under indicated conditions. Reads representing spliced or unspliced

XBP1 mRNA were identified based on the presence or absence of the 26 nucleotide intron and quantified. (D-I) Percentage of XBP1 spliced reads, or relative expression of total XBP1 and DNAJB9 mRNA from the RNA-seq samples were then plotted. Values are means ± SD (error bars). Statistical significance was determined by Unpaired t-tests (* = P < 0.05; ** = P < 0.01; ns = not significant).

Figure 5: SARS-CoV-2 and MERS-CoV induce IRE1α phosphorylation in iAT2 cells but diverge in induction of XBP1 splicing.

iPSC-derived AT2 cells (iAT2 cells) were mock infected or infected (in triplicate) with MERS-CoV or SARS-CoV-2 at a MOI of 5. (A) At the indicated timepoints, supernatants were collected and infectious virus quantified by plaque assay. Values are means ± SD (error bars). Statistical significance was determined by two-way ANOVA (* = P < 0.05; ns = not significant). (B) Total protein was harvested at the indicated timepoints and analyzed by immunoblotting using the indicated antibodies. Thapsigargin treatment for 1 hour (Tg; 1μM) was used as a positive control for IRE1α activation while DMSO served as a vehicle control. (C) Total RNA was harvested at the indicated timepoints and relative %XBP1s, XBP1s, total XBP1 and DNAJB9 mRNA expression were quantified by RT-qPCR, calculated, and displayed as described above. Values are means ± SD (error bars). Statistical significance (infected compared to mock) were determined using two-tailed, paired Student *t*-test. Displayed significance is determined by p-value (P), where * = P < 0.05; ** = P < 0.01; *** = P < 0.001; **** = P < 0.0001; ns = not significant. (D) RT-PCR was performed using extracted RNA and primers crossing the XBP1 splicing site. The product was run an on an agarose gel to visualize XBP1 splicing. Tunicamycin treatment (1μg/mL for 6 hours) was used as a positive control for RT-(q)PCR, while DMSO treatment served as a vehicle control. Data shown are from one representative experiment from at least two independent experiments.

Figure 6: SARS-COV-2 inhibits IRE1α-medicated XBP1 splicing under ER stress and does not require IRE1α for replication.

(A&B) A549-ACE2 cells were mock infected or infected (in triplicate) with SARS-CoV-2 (MOI=3) (A) or OC43 (MOI=1) (B) for 24 hours prior to treatment with low doses of tunicamycin (100-175 ng/mL) for 6 hours. Total RNA was harvested and used to quantify the relative %XBP1s and XBP1s expression by RT-qPCR. C_T values were normalized to 18S rRNA and expressed as fold-change over mock displayed as $2^{-\Delta(\Delta Ct)}$. Technical replicates were averaged, the means for each replicate are displayed as ±SD (error bars). Statistical significance (infected compared to mock) was determined by one-tailed, paired t-tests (* = P < 0.05; ** = P < 0.01; *** = P < 0.001; ns = not significant). (C-F) Infection of CRISPR/Cas9-edited IRE1α KO A549 cells with different coronaviruses. Experiments were performed using sgControl or IRE1α KO or XBP1 KO (where indicated) A549 cells stably expressing viral receptors: A549-ACE2 (OC43 or SARS-CoV-2), A549-DDP4 (MERS-CoV) and A549-MHVR (MHV). Cells were infected (in triplicate) with SARS-CoV-2, MERS-CoV, OC43, or MHV at a MOI of 1. At the indicated times, supernatants were collected and infectious virus quantified by plaque assay. Values are means ± SD (error bars). Statistical significance was determined by two-way ANOVA (* = P < 0.05; ** = P < 0.01; ns = not significant). Data shown are from one representative of at least two independent experiments. (G) Model of MHV, OC43 and MERS-CoV infection activating IRE1α/ XBP1 pathway compared to SARS-CoV-2 that induces IRE1α autophosphorylation but not IRE1α RNase mediated XBP1 splicing.

Supplemental Figure 1. Kinetics of activtion of IRE1α phosphorylation during infection with MERS-CoV or SARS-CoV-2.

(A-B) A549 cells expressing the indicated viral receptors were mock infected or infected with MERS-CoV (A) or SARS-CoV-2 (B) at a MOI of 5. At the indicated timepoints, protein was harvested and analyzed by immunoblotting with indicated antibodies. Cells treated with thapsigargin (Tg, 1μM) for 1 hour or tunicamycin (TM, 1μg/ mL) for 8 hours or were used as a positive control for IRE1α phosphorylation and attenuation, respectively. Data shown are from one representative experiment from at least two independent experiments.

Supplemental Figure 2. XBP1 is spliced in MHV infected cells

(A) Schematic of method and primer design used to quantify %XBP1. (B) A549-MHVR cells were mock infected or infected with MHV (MOI=0.1). Total RNA was harvested at 48 hours post infection. Relative %XBP1s, XBP1s, total XBP1 and DNAJB9 mRNA expression were quantified by RT-qPCR. C_T values were normalized to 18S rRNA and expressed as fold-change over mock displayed as $2^{-\Delta(\Delta Ct)}$. Technical replicates were averaged, the mean for each biological replicate (n=2) is displayed, ±SD (error bars).

Supplemental Figure 3. Validation of IRE1α and XBP1 knockout cell lines using CRISPR/Cas9. (A-C) A549 cells expressing the indicated viral receptors subjected to CRISPR/Cas9 editing using different guide RNAs targeting IRE1α were immunoblotted for IRE1α protein to assess knockout efficiency. (D) CRISPR/Cas-9 gene edited IRE1α KO A549-ACE2 cell lines were treated with tunicamycin (500 ng/mL) or DMSO for 6 hours. Total RNA was harvested and %XBP1 quantified by RT-qPCR. Technical replicates were averaged, the means for each replicate displayed. Data shown are one representative experiment from at least three independent experiments. (E) CRISPR/Cas9 gene edited IRE1α KO A549-ACE2 (guide 3) or control A549-ACE2 were treated with tunicamycin (Tm, 1μg/mL) for 8 hours. Total RNA was harvested and amplied for XBP1. XBP1 cDNA product was assayed on agarose gel to visualize

splicing. (F) Control or IRE1α KO A549-DDP4 cells were infected with MERS-CoV (MOI=1). At the indicated time points, total RNA was collected. RT-PCR was performed using primers crossing the XBP1 splicing site. The product was analyzed on an agarose gel to visualize XBP1 splicing. (G) CRISPR/Cas9 gene edited control or XBP1 KO A549-ACE2 were treated with DMSO or tunicamycin (Tm, 1μg/mL) for 6 hours. Lysates were then immunblotted for XBP1s to confirm knockout efficiency.

Figure 1

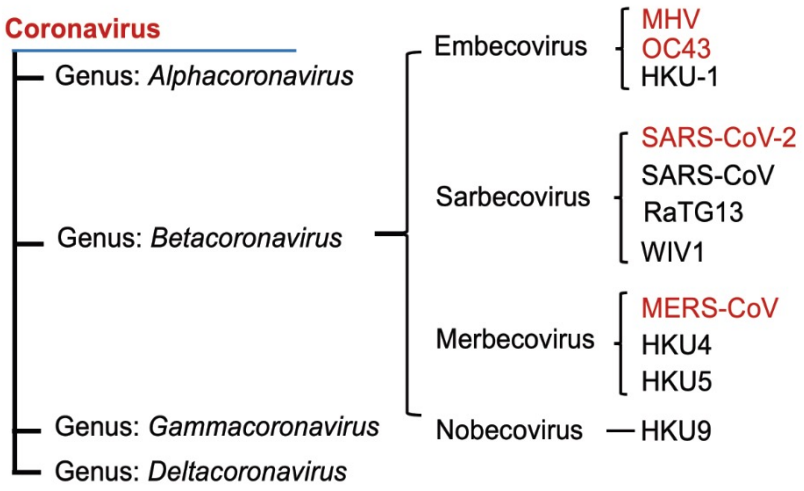
Coronavirus
Genus: Alphacoronavirus
Genus: Betacoronavirus
Genus: Gammacoronavirus
Genus: Deltacoronavirus
Embecovirus
MHV
OC43
HKU-1
Sarbecovirus
SARS-CoV-2
SARS-CoV
RaTG13
WIV1
Merbecovirus
MERS-CoV
HKU4
HKU5
Nobecovirus
HKU9

Figure 2

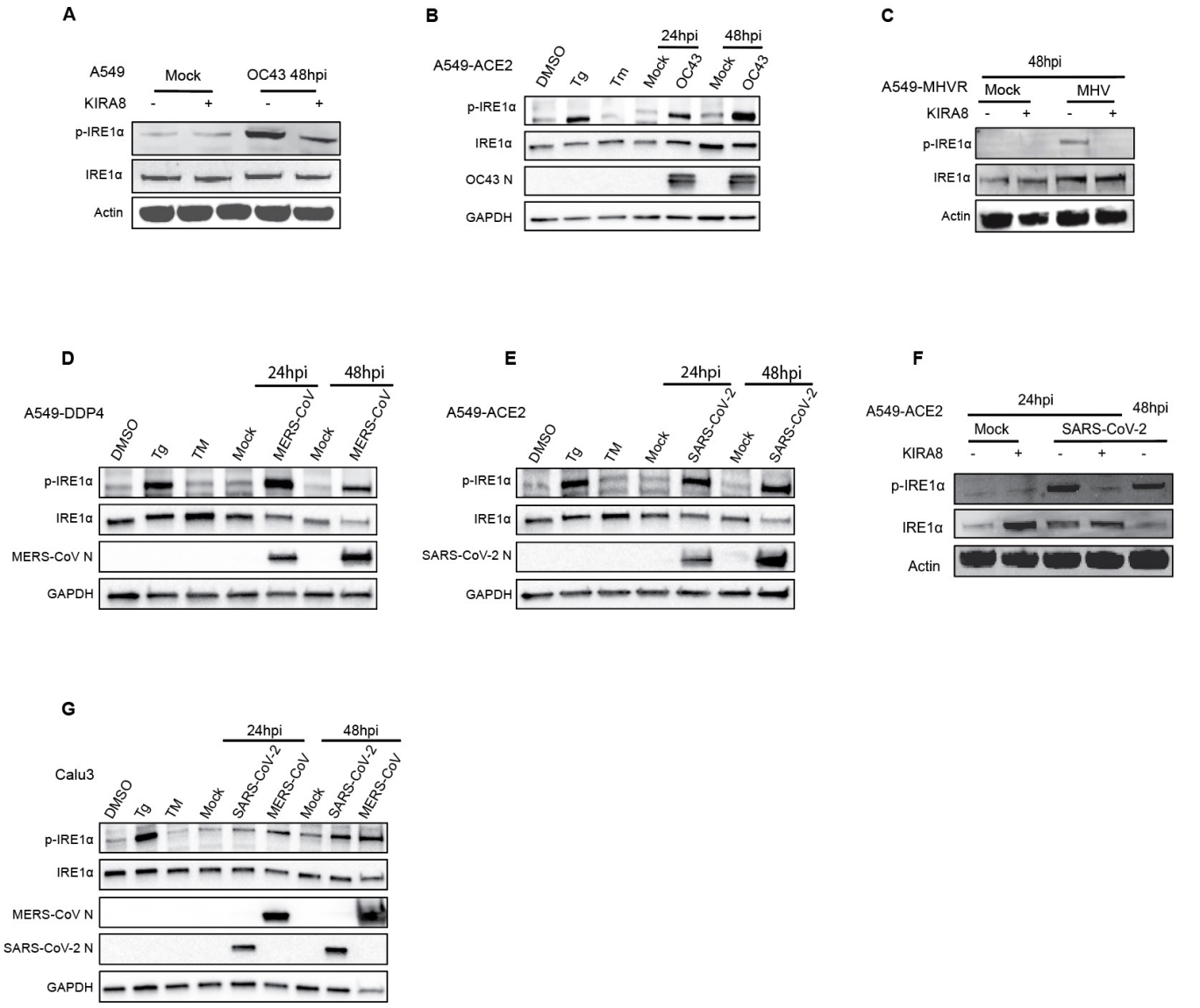
A
A549
Mock
OC43 48hpi
KIRA8
- + - +
p-IRE1α
IRE1α
Actin
B
A549-ACE2
24hpi
48hpi
DMSO
Tg
Tm
Mock
OC43
Mock
OC43
p-IRE1α
IRE1α
OC43 N
GAPDH
C
A549-MHVR
48hpi
Mock
MHV
KIRA8
- + - +
p-IRE1α
IRE1α
Actin
D
A549-DDP4
24hpi
48hpi
DMSO
Tg
TM
Mock
MERS-CoV
Mock
MERS-CoV
p-IRE1α
IRE1α
MERS-CoV N
GAPDH
E
A549-ACE2
24hpi
48hpi
DMSO
Tg
TM
Mock
SARS-CoV-2
Mock
SARS-CoV-2
p-IRE1α
IRE1α
SARS-CoV-2 N
GAPDH
F
A549-ACE2
24hpi
48hpi
Mock
SARS-CoV-2
KIRA8
- + - + -
p-IRE1α
IRE1α
Actin
G
Calu3
24hpi
48hpi
DMSO
Tg
TM
Mock
SARS-CoV-2
MERS-CoV
Mock
SARS-CoV-2
MERS-CoV
p-IRE1α
IRE1α
MERS-CoV N
SARS-CoV-2 N
GAPDH

Figure 3

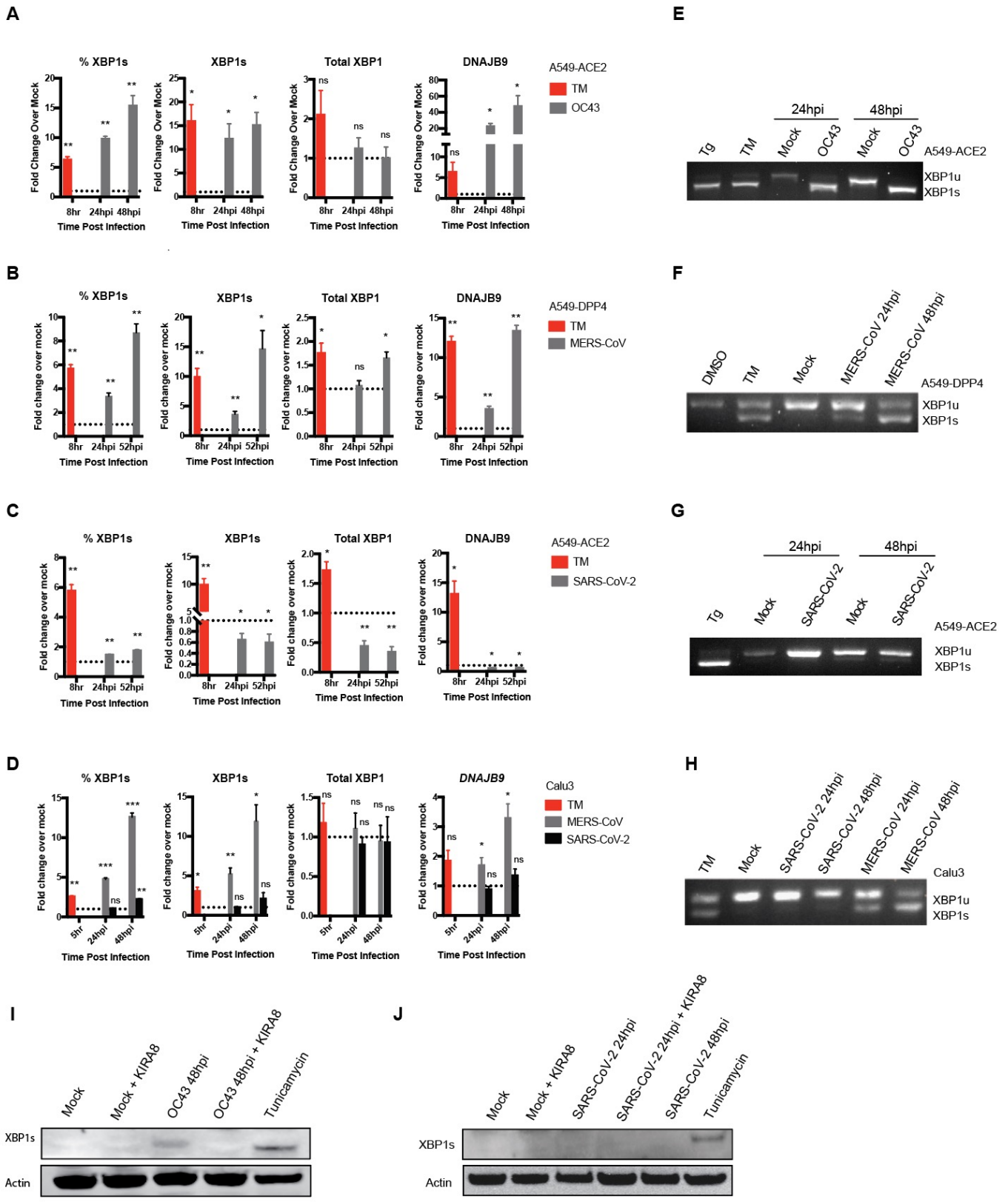
A
% XBP1s
XBP1s
Total XBP1
DNAJB9
Fold Change Over Mock
Time Post Infection
8hr
24hpi
48hpi
A549-ACE2
TM
OC43
B
Fold change over mock
52hpi
A549-DPP4
MERS-CoV
C
SARS-CoV-2
D
Calu3
5hr
E
24hpi
48hpi
Tg
Mock
XBP1u
XBP1s
F
DMSO
MERS-CoV 24hpi
MERS-CoV 48hpi
G
H
SARS-CoV-2 24hpi
SARS-CoV-2 48hpi
I
Mock + KIRA8
OC43 48hpi
OC43 48hpi + KIRA8
Tunicamycin
Actin
J

Figure 4

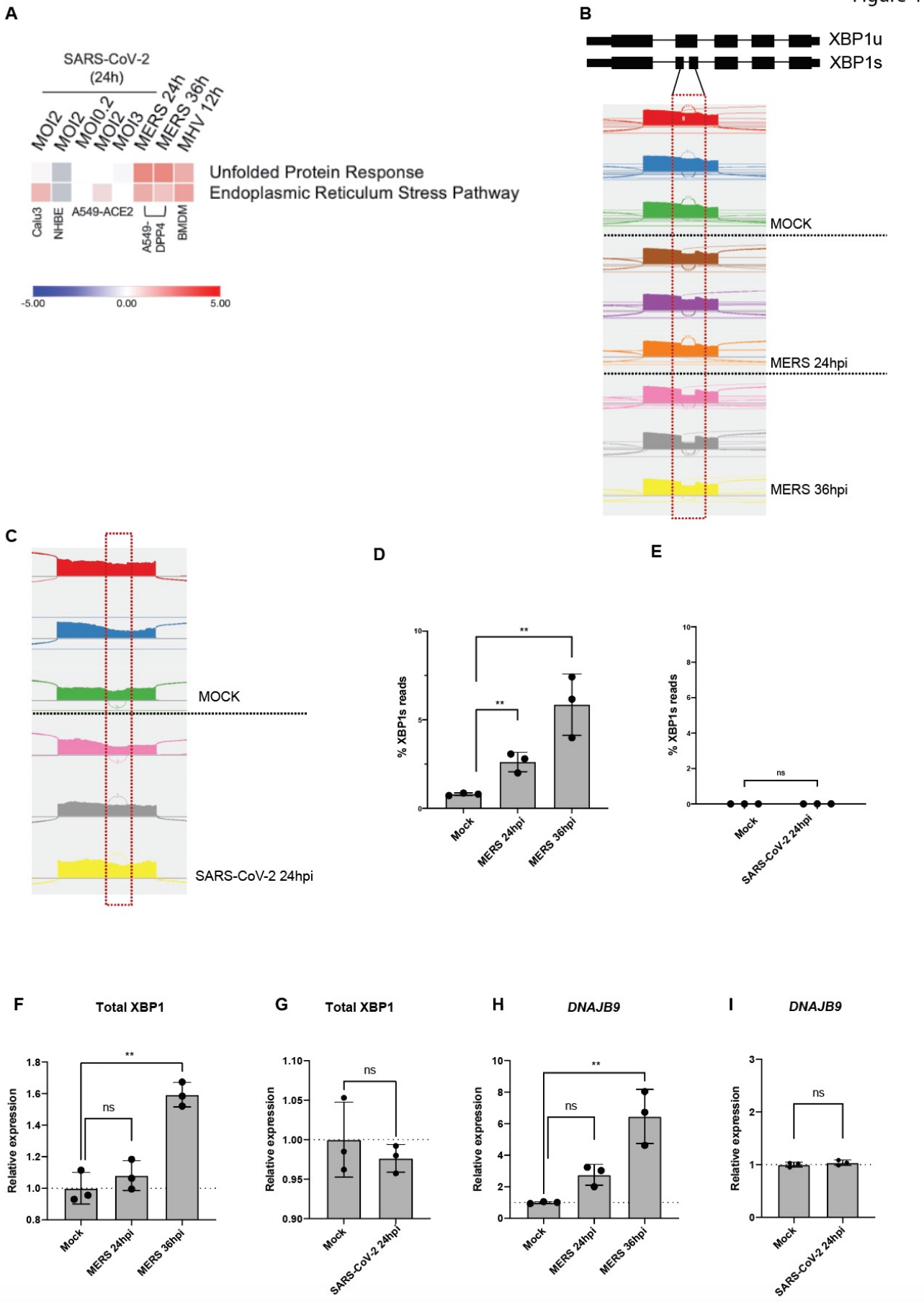
A
SARS-CoV-2 (24h)
MOI2
MOI2
MOI0.2
MOI2
MOI3
MERS 24h
MERS 36h
MHV 12h
Unfolded Protein Response
Endoplasmic Reticulum Stress Pathway
Calu3
NHBE
A549-ACE2
A549-DPP4
BMDM
-5.00
0.00
5.00
B
XBP1u
XBP1s
MOCK
MERS 24hpi
MERS 36hpi
C
MOCK
SARS-CoV-2 24hpi
D
% XBP1s reads
Mock
MERS 24hpi
MERS 36hpi
E
% XBP1s reads
ns
Mock
SARS-CoV-2 24hpi
F
Total XBP1
Relative expression
ns
Mock
MERS 24hpi
MERS 36hpi
G
Total XBP1
Relative expression
ns
Mock
SARS-CoV-2 24hpi
H
DNAJB9
Relative expression
ns
Mock
MERS 24hpi
MERS 36hpi
I
DNAJB9
Relative expression
ns
Mock
SARS-CoV-2 24hpi

Figure 5

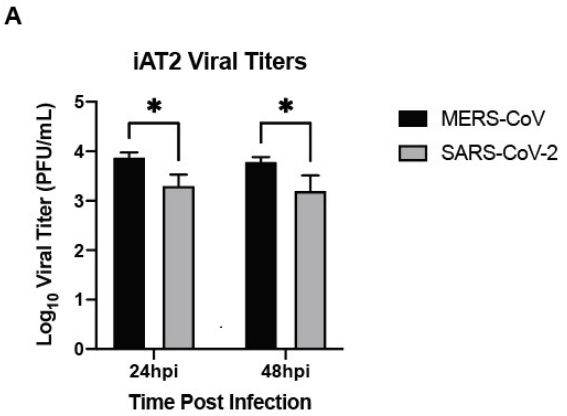
A
iAT2 Viral Titers
Log10 Viral Titer (PFU/mL)
5
4
3
2
1
0
*
*
24hpi
48hpi
Time Post Infection
MERS-CoV
SARS-CoV-2

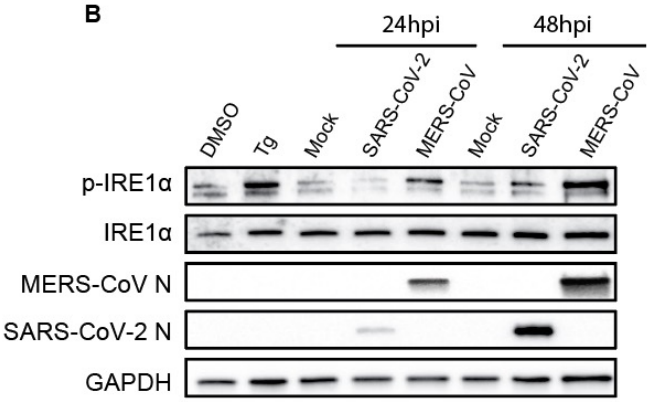
B
24hpi
48hpi
DMSO
Tg
Mock
SARS-CoV-2
MERS-CoV
Mock
SARS-CoV-2
MERS-CoV
p-IRE1α
IRE1α
MERS-CoV N
SARS-CoV-2 N
GAPDH

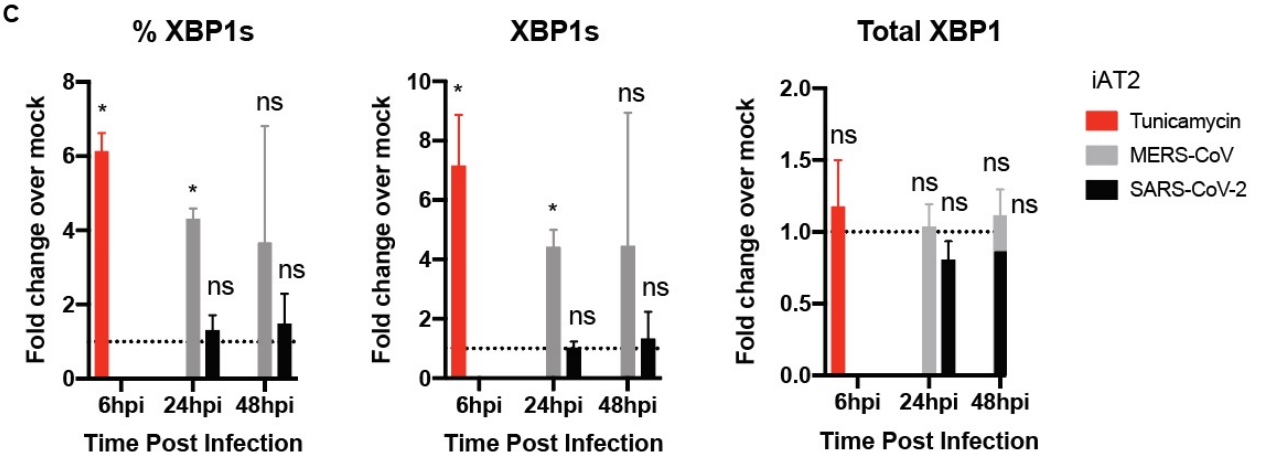
C
% XBP1s
XBP1s
Total XBP1
Fold change over mock
Time Post Infection
6hpi
24hpi
48hpi
ns
*
iAT2
Tunicamycin
MERS-CoV
SARS-CoV-2

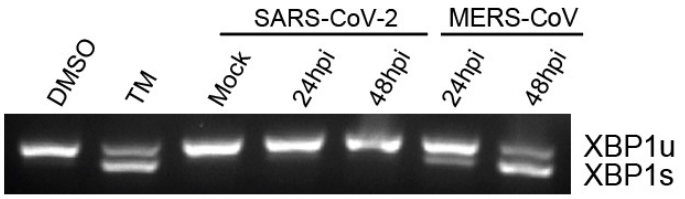
D
SARS-CoV-2
MERS-CoV
DMSO
TM
Mock
24hpi
48hpi
24hpi
48hpi
XBP1u
XBP1s

Figure 6

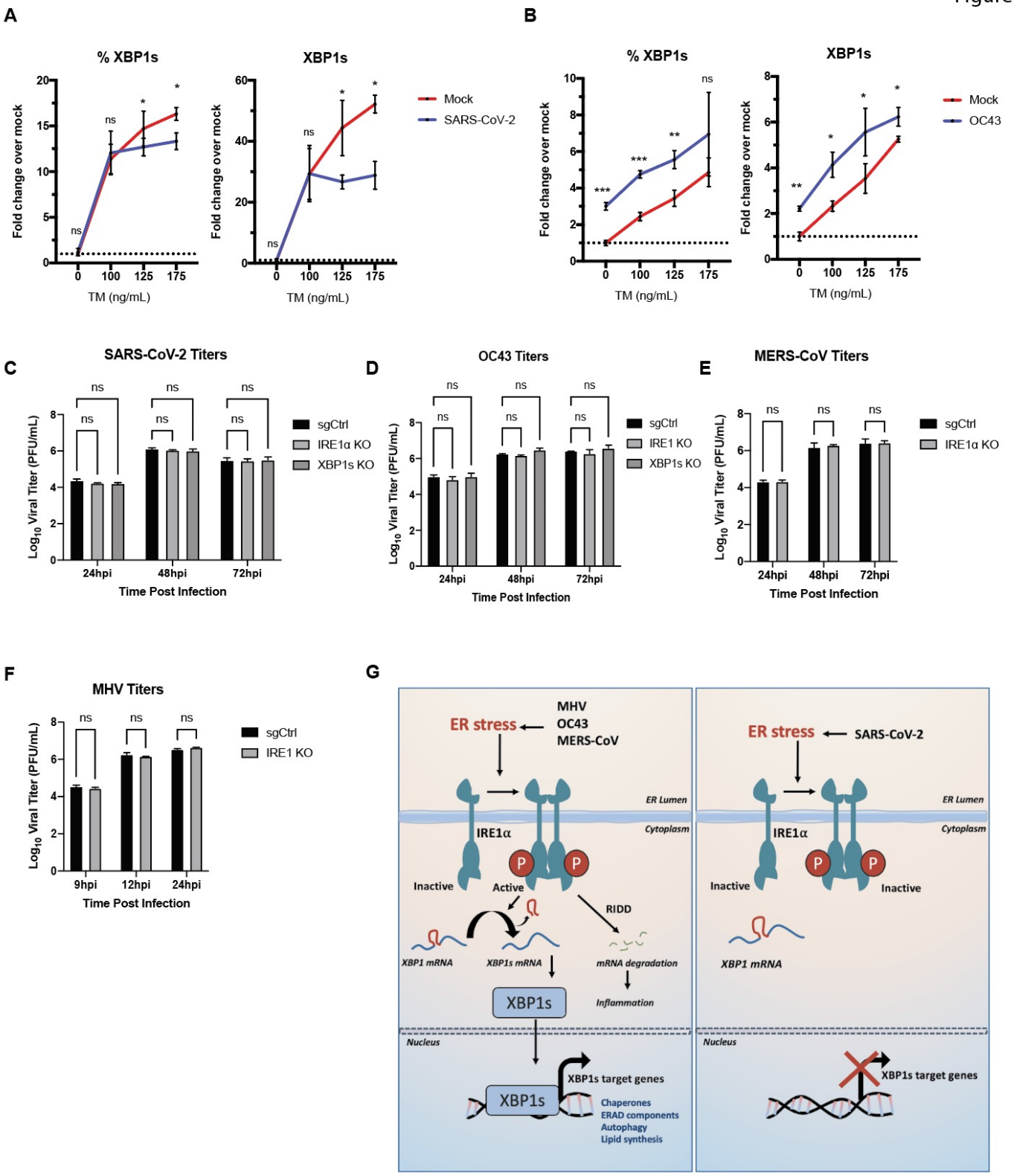
A
% XBP1s
XBP1s
Fold change over mock
TM (ng/mL)
Mock
SARS-CoV-2
B
% XBP1s
XBP1s
Mock
OC43
C
SARS-CoV-2 Titers
D
OC43 Titers
E
MERS-CoV Titers
Log10 Viral Titer (PFU/mL)
Time Post Infection
24hpi
48hpi
72hpi
sgCtrl
IRE1α KO
XBP1s KO
IRE1 KO
F
MHV Titers
9hpi
12hpi
24hpi
G
ER stress
MHV
OC43
MERS-CoV
SARS-CoV-2
ER Lumen
Cytoplasm
IRE1α
Inactive
Active
RIDD
XBP1 mRNA
XBP1s mRNA
mRNA degradation
Inflammation
XBP1s
Nucleus
XBP1s target genes
Chaperones
ERAD components
Autophagy
Lipid synthesis

Supplement Figure 1

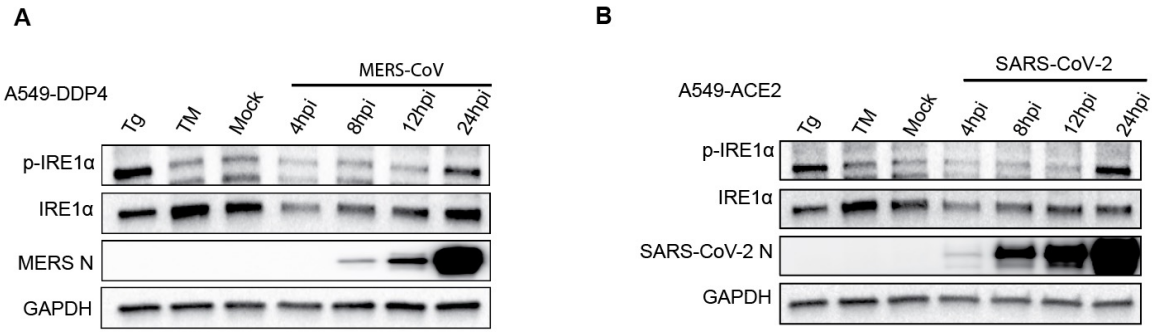

Supplement Figure 2

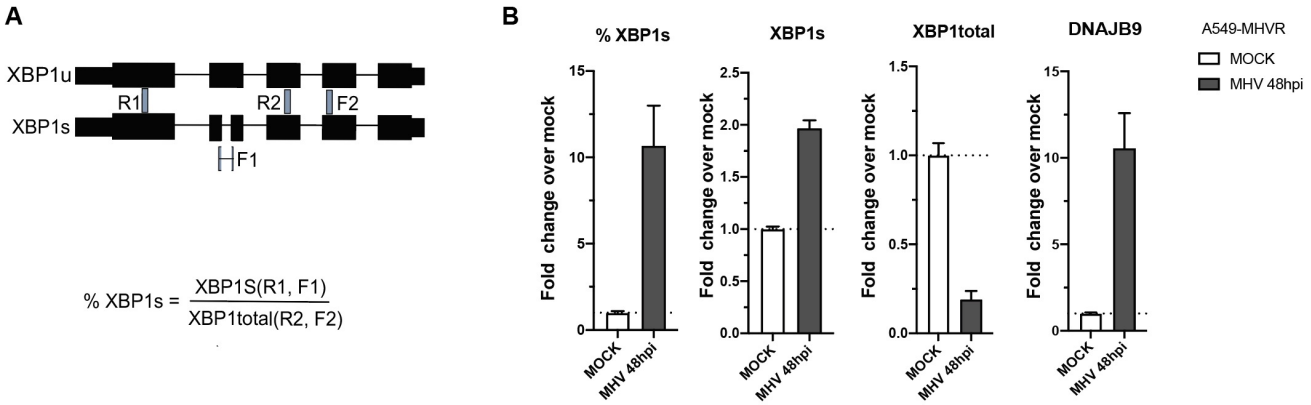
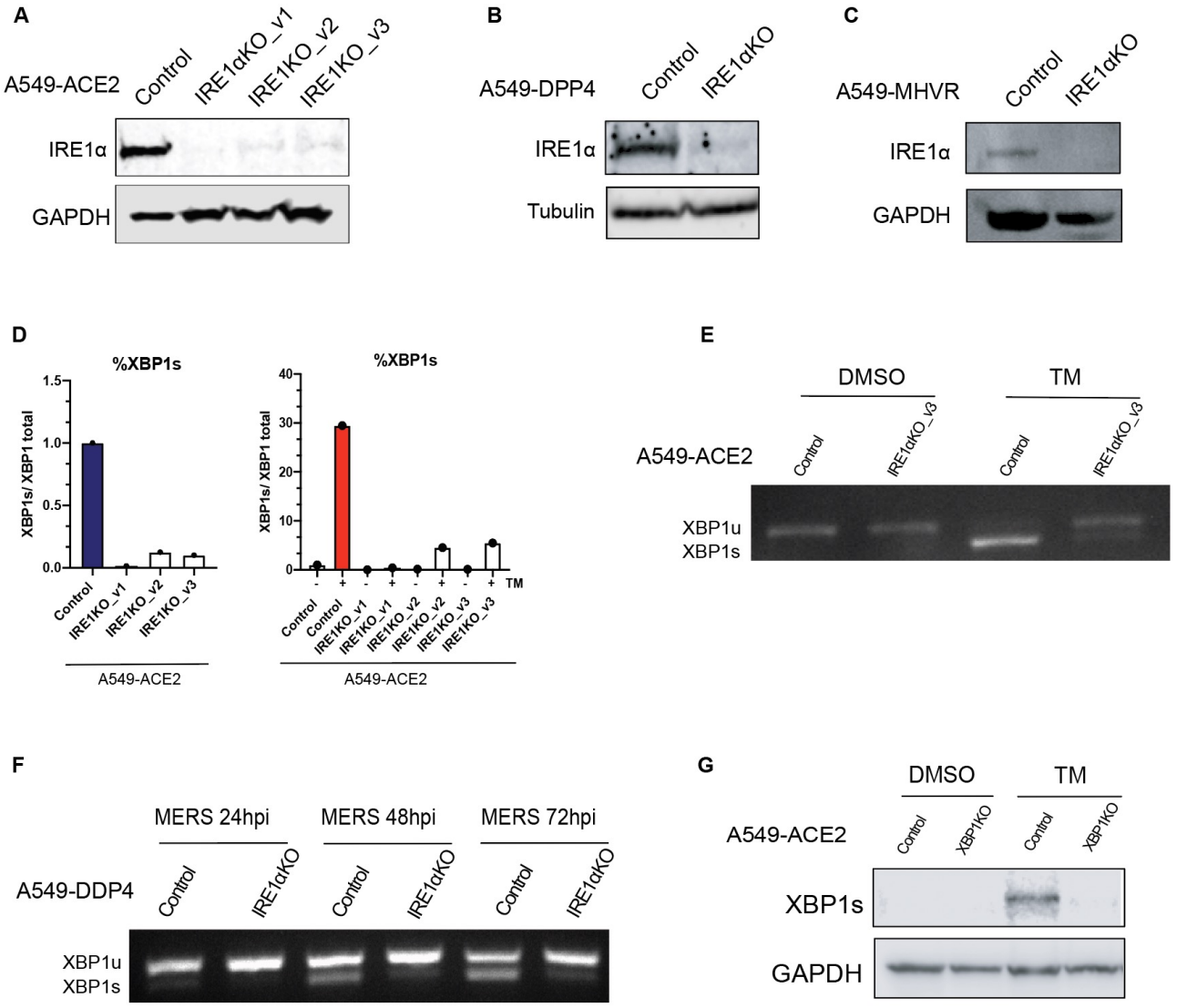
Supplement Figure 3